Int J Adv Manuf Technol (2015) 80:1015–1026
DOI 10.1007/s00170-015-7061-y

ORIGINAL ARTICLE

Forming limit of local loading forming of Ti-alloy large-scale rib-web components considering defects in the transitional region

Pengfei Gao[1] · **He Yang**[1] · **Xiaoguang Fan**[1] · **Penghui Lei**[1]

Received: 31 October 2014 / Accepted: 18 March 2015 / Published online: 12 April 2015
© Springer-Verlag London 2015

Abstract The forming quality in the transitional region largely determines the formability of local loading forming of the large-scale rib-web component. Thus, it is very critical to determine the forming limit considering defects in the transitional region during local loading forming. In this paper, the stepwise searching method based on Kriging metamodels of defect indexes is adopted to determine the above forming limit. First, the finite element (FE) simulation of the transitional region during local loading forming and the evaluation indexes for folding and cavum defects are introduced. Then, the Kriging metamodels of defect indexes are developed based on quantities of FE simulation results under various geometry parameters. During Kriging metamodeling, in order to guarantee the accuracy of the metamodel in the global design space and interesting region simultaneously, the space-filling maximin Latin hypercube designs (maximin LHDs) and sequential sampling approach are employed to design sample points. After metamodeling, extra random samples designed within the whole space are simulated to validate the developed Kriging metamodels. At last, the method of determining the forming limit considering defects in the transitional region is presented and applied to two specific transitional region models. It is realized through stepwise searching based on Kriging metamodels of defect indexes. The application results show that the proposed method is an effective and reliable method to determine the forming limit considering defects in the transitional region. It would provide an important guideline in the processing design of local loading forming of titanium alloy large-scale rib-web components.

Keywords Local loading forming · Large-scale rib-web component · Defects in transitional region · Forming limit

1 Introduction

The large-scale rib-web components of titanium alloy (such as bulkhead) have been widely used in the aerospace field as key lightweight load-bearing components [1–5]. However, it is difficult to form this kind of component due to the complexity of the shape and the hard-working property of titanium alloy. The isothermal local loading forming technique (Fig. 1), in which a load is applied to part of the billet and the component is formed by changing the loading region, provides a new approach to form these components [6–9]. However, during local loading forming, the transitional region undergoes complicated uneven plastic deformation under the constraints of the loading and unloading regions. It may lead to some forming defects such as folding and underfilling, thus weakening the forming accuracy and performance. So, how to prevent the defects of the transitional region is one of the main challenges in local loading forming of large-scale rib-web components.

By now, some studies have been conducted on the mechanisms of material flow and defect formation in the transitional region during local loading forming of large-scale rib-web components. Zhang et al. [10] found that there exists some material flowing into the unloaded area from the loaded area due to the local loading characteristic, and it may cause some defects in the transitional region. Zhang and Yang [11] further qualitatively studied the distribution of metal flowing from the loading area into the unloading area. In addition, Gao et al. [8]

✉ He Yang
yanghe@nwpu.edu.cn

[1] State Key Laboratory of Solidification Processing, School of Materials Science and Engineering, Northwestern Polytechnical University, P.O. Box 542, Xi'an 710072, People's Republic of China

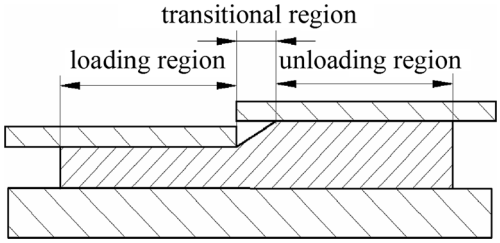

Fig. 1 Illustration of the local loading forming [6]

quantitatively investigated the material flow mechanism of the transitional region during local loading forming. These works on material flow provide helpful basis for the study of the defect mechanism in the transitional region. Gao et al. [12] investigated the mechanism of forming defects in the transitional region and their dependences on processing parameters by the combination of physical experiment and finite element (FE) simulation. The results show that folding and cavum defects are prone to emerge in the transitional region during local loading forming of the rib-web component, as shown in Fig. 2. It is suggested that decreasing the thickness of the spacer block and increasing the friction both can suppress these defects, while the latter plays a much smaller role than the former. So, decreasing the spacer block thickness becomes the most efficient way to suppress the forming defects of the transitional region. Considering the precondition in local loading forming that the spacer block thickness (H_{sb})≥the reduction amount (L) in each loading pass, H_{sb} is usually optimally set equal to L. Above, it can be concluded that a smaller reduction amount is beneficial to preventing the forming defects in the transitional region. However, it would increase the loading pass then raise the production costs and prolong the production cycle. Moreover, in multi-pass local loading forming, the workpiece would undergo series of thermal cycles (heating, holding, deformation, and cooling), which may result in bad microstructure and poor performance. Thus, it is of great significance to maximize the reduction amount in each loading pass in the precondition of guaranteeing forming quality of the transitional region. But, there is still a lack of corresponding design criteria for the reduction amount in local loading forming now. Therefore, further investigation is needed to determine the maximum reduction amount with the qualified transitional region, called forming limit here, during the local loading forming of large-scale rib-web components.

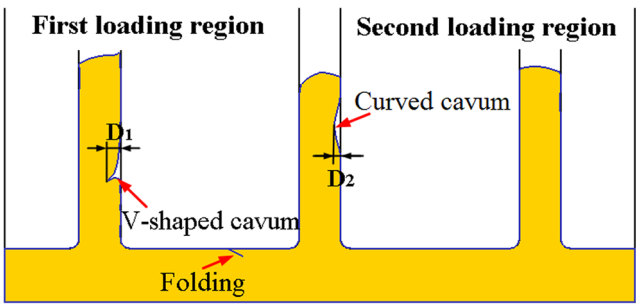

Fig. 2 Usual defects of transitional region in local loading forming of large-scale rib-web component

As for the method of determining the forming limit, stepwise searching with a small interval is a very easy and effective method, which has been already used successfully in other forming processes. Chen et al. [13] studied the flow-through phenomenon that occurred in press forging of AZ31 magnesium-alloy sheets by FE simulation, and revealed that an increasing sheet thickness could suppress the occurrence of flow-through. Then, they found the least sheet thickness that could prevent the flow-through for a specific embossment dimension through the stepwise searching method. Sun and Yang [14] found that in the tube axial compressive process with a conical die, a larger half conical angle of the die could suppress the tearing defect, while a smaller half conical angle could suppress the buckling defect. Then, they also applied the stepwise searching method based on FE simulation to determine the minimum and maximum half conical angles that could avoid the tearing and buckling defect, respectively. However, in the above works, the stepwise searching based on FE simulation demands quantities of time-consuming simulations. Especially for problems with various geometric parameters, the corresponding FE models must be established and computed repeatedly, which makes the determination of the forming limit tedious, inefficient, and high cost. Fortunately, the metamodel technique can approximate the computation-intensive FE simulation with simple analytical models, thereby improving the overall computation efficiency [15–17]. Specially, the Kriging metamodel is gaining popularity in approximating deterministic computer models. It interpolates the observed or known data points and covers the whole experimental space, thus often giving better global predictions than regression analysis [18–21]. Therefore, using the stepwise searching method based on a fitted Kriging metamodel provides a feasible way to quickly determine the forming limit.

In this paper, the FE simulation of the transitional region and evaluation indexes of defects in the transitional region during local loading forming of large-scale rib-web component are introduced in Section 2. Then, the Kriging metamodels of defect indexes are developed in Section 3. It consists of experiment design by sequential sampling, Kriging metamodel fitting based on simulation results, and metamodel validation. At last, the method and cases for determining the forming limit of local loading forming considering defects in the transitional region are presented in Section 4. The results would provide an important guideline in the processing design of local loading forming of titanium alloy large-scale rib-web components.

2 FE simulation of the transitional region in local loading forming

In previous studies [8, 12, 22], a local eigen model of the transitional region in local loading forming of a large-scale rib-web component was extracted, and its corresponding simplified 2D FE model (Fig. 3 [22]) was established to study the mechanisms of material flow and defects formation in the transitional region. As shown in Fig. 3, the top die is separated into two parts: top die 1 and top die 2, while the lower die is kept integral. The local loading forming is carried out by one or more loading passes and each loading pass includes two loading steps. In the first loading step, the billet under top die 1 deforms locally, which is achieved by implanting a spacer block between top die 1 and the top die bed. It should be noted that the thickness of the spacer block (H_{sb}) should be equal to or larger than the reduction amount (L), as mentioned above. Otherwise, it would cause a large forming load when the stroke exceeds H_{sb} in the first loading step, as the whole component would contact the top dies and be loaded. It can be regarded as integral forging in this stage, which is against the idea of saving the load of local loading forming. Thus, in local loading forming, $H_{sb} \geq L$ is required. In the second loading step, the spacer block is removed with top die 1 and top die 2 being at the same level. The structural feature of the transitional region can be expressed by the following characteristic parameters: a_{01}, a_{12}, a_{23}, a_{30}, b_1, b_2, b_3, billet height (H), and L, as shown in Fig. 3a, b. The fillet radius is 3 mm. In FE modeling, the billet deformation is modeled as a rigid-plastic type with the material model of TA15 alloy in [23], while the punch and die are modeled as rigid bodies. The local loading forming is modeled in an isothermal condition without any thermal events. The von Mises yielding criteria and shear friction model are employed. Besides, the local refined meshing and automatic remeshing techniques are used to avoid meshing-induced singularity. The developed FE model has been verified to be reliable to predict the formation of folding and cavum depths in the transitional region by physical experiments in previous works [8, 12, 22]. Thus, this FE model is used here to predict the forming defects of the transitional region under different conditions, providing essential data for Kriging metamodeling.

Primary study shows that the structural parameters have great influence on the forming defects of the transitional region. So, the forming limit may also strongly depend on the structural parameters. Thus, the objective of this work is to determine the forming limit for local loading forming of rib-web components with various structural parameters. Table 1 gives the structural parameters of the transitional region and processing parameters in this work. The structural parameters are determined referring to the common structure parameters of the titanium alloy rib-web component [24]. Considering forming quality, the optimal processing conditions, i.e., $H_{sb}=L$ and largest possible friction (0.5), are taken. The deformation temperature and loading speed are prescribed as 950 °C and 0.1 mm/s, respectively.

In the analysis of FE simulation results, the V-shaped and curved cavum defects are evaluated by their depths, noted as D_1 and D_2, respectively, as shown in Fig. 2. The cavum depth is employed as the response in the subsequent Kriging metamodeling of the cavum defect. However, whether the folding defect (Fig. 2) is generated or not is a qualitative index, which can be observed visually in the FE simulation but cannot be used as a response in the Kriging metamodel. To address such a challenge, an adaptive folding index that can evaluate the possibility of folding and the corresponding judging criterion for the folding defect were proposed in a previous work [22]. Thus, the folding defect can be evaluated expediently through establishing a Kriging metamodel of the folding index combined with the corresponding judging criterion. The folding index and its corresponding judging criterion are introduced and verified in detail in [22], which are just described briefly in this work. The adaptive folding index is given as follows, which is calculated via the user subroutine of the DEFORM software:

$$\varphi_{\text{fold}} = \int_{t_0}^{t_{\text{fold}}} \left(\frac{1}{\int_{\partial\Omega_{\text{foldzone}}} ds} \frac{s_{\text{ref}}}{s_{\text{ave}}} \int_{\partial\Omega_{\text{foldzone}}} \dot{\bar{\varepsilon}} ds \right) dt \qquad (1)$$

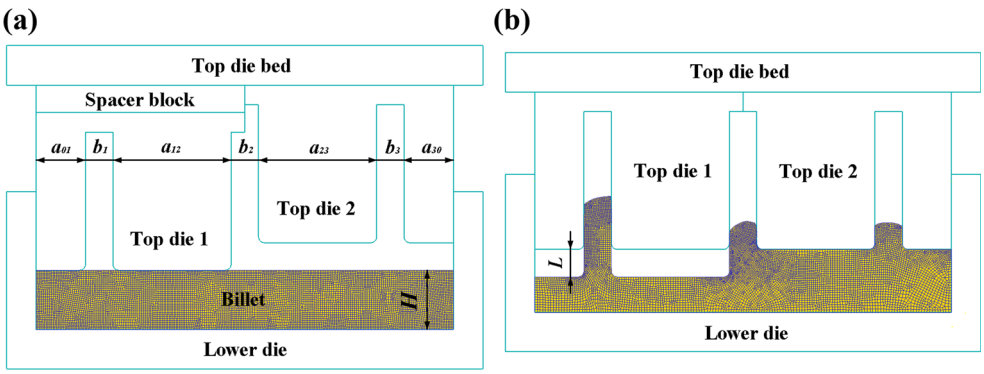

Fig. 3 2D FE model of transitional region in local loading forming of large-scale rib-web component. **a** The first loading step; **b** the second loading step [22]

Table 1 Structural and processing parameters of the transitional region model in the local loading forming of TA15 titanium alloy

	Parameter	Range
Feature parameters	a_{01}	20–50 mm
	a_{12}	40–100 mm
	a_{23}	40–100 mm
	a_{30}	20–50 mm
	b_1	12–18 mm
	b_2	12–18 mm
	b_3	12–18 mm
	Billet height (H)	20–30 mm
	Reduction amount (L)	5–11 mm
Processing parameters	Spacer block thickness (H_{sb})	H_{sb}=L
	Friction factor (m)	0.5
	Loading speed	0.1 mm/s
	Deformation temperature	950 °C

where t_0 is the initial time of the second loading step, t_{fold} is the time when the development of the folding defect is finished, $\partial\Omega_{foldzone}$ is the free surface in the folding zone, s_{ref} (reference value of area) is taken as 1, $s_{ave} = \frac{1}{nbelt}\sum_{1}^{nbelt} s_i$, nbelt is the number of free surface elements in the folding zone, and s_i is the area of element. The folding zone is determined based on previous works [8, 12], in which the production and evolution mechanisms of the folding defect were revealed. It is found that the folding defect is prone to be produced at the left of the middle rib. And, its related zone is located in a 15-mm-wide zone at the left of the step for samples with our interested structural parameters (Table 1). Therefore, the folding zone is determined accordingly, as shown in Fig. 4. Note that the folding zone would move during the forming process. Considering the safety margin in engineering application, the critical value of the folding index for judging folding is taken as 17.5. If the folding index is ≤17.5, it is judged as no folding defect is occurring; when the index is >17.5, it is judged as the folding defect is occurring. The critical value of the folding index was determined as follows. First, we checked the availability of the folding index to evaluate the possibility and severity of the folding defect. Then, the relationship between the folding defect and the folding index was given based on quantities of uniform experiments. According to this relationship, the critical value can be determined. At last, the critical value of the folding index for judging the folding defect was validated by some random samples. It should be noted that the critical value is conservatively taken as 17.5, considering the safety margin in this work, which deviates a little from the value in [22].

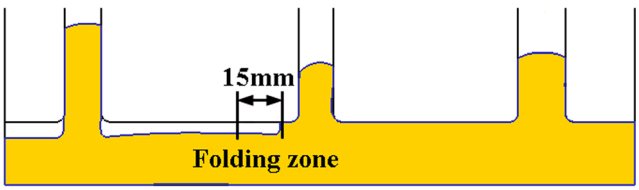

Fig. 4 Schematic diagram of folding zone [22]

3 Kriging metamodeling

Metamodel techniques are becoming widely used in engineering to minimize the computational expense of running computer analyses. The basic approach is to construct approximations of the computation-intensive simulations to provide surrogate models with sufficient accuracy to replace the original simulations. It can facilitate the design space exploration, product and process optimization, and reliability analysis to a very great extent [15, 25]. A variety of metamodel techniques exist for constructing surrogate models of tedious computer simulations, such as response surface methodology (RSM), radial basis function (RBF), and Kriging model. Systematic comparative studies have been conducted and reviewed on the performance of various metamodel techniques under different modeling criteria [15, 16, 25–28]. However, it is difficult to draw a conclusion about which model is definitely superior to the others. The RSM model is originally developed to analyze the physical experiment results and create an empirically based model of the response values. It is based on fitting a lower order polynomial metamodel through response points. It is easy to construct and clear on parameter sensitivity, and allows for a random error, while it is inappropriate to model highly nonlinear or irregular behaviors. Moreover, using RSM for approximating deterministic computer analyses is statistically questionable because of the lack of a random error in the computer model [15, 25, 28]. The RBF model is an interpolating approximation, which uses linear combinations of a radially symmetric function based on Euclidean distance or similar metric to construct metamodels. It can provide good accuracy for fitting highly nonlinear behaviors. However, it cannot provide the estimation of a prediction error, which restricts its application in some sequential sampling approaches [26–28]. The Kriging method provides an "exact" interpolation, i.e., predicted output values at observed input points equal the simulated values. Such interpolation is attractive in deterministic simulation and is often applied in computer-aided engineering. Methodologically, a Kriging metamodel covers the whole experimental area; i.e., it is global and often gives better global predictions than regression analysis. In addition, the Kriging method is extremely flexible because of the wide range of correlation functions that have a small amount of unknown coefficients. Besides, it can provide accurate predictions of highly nonlinear or irregular behaviors.

Table 2 Simulation schemes and results of 51 samples designed by the maximin LHDs

Sample	a_{01} (mm)	a_{12} (mm)	a_{23} (mm)	a_{30} (mm)	b_1 (mm)	b_2 (mm)	b_3 (mm)	H (mm)	L (mm)	φ_{fold}	D_1 (mm)	D_2 (mm)
1	20	65.2	54.4	41.6	13.44	15	12.72	27.2	5.72	9.420	0.64	1.56
2	20.6	52	90.4	44.6	16.68	15.72	14.4	21.4	8.96	23.700	2.32	2.89
3	21.2	91.6	89.2	37.4	15.96	13.56	12.6	27.4	9.2	20.129	1.5	1.66
4	21.8	82	85.6	42.2	12.48	17.64	16.2	25.8	8.84	20.589	1	2.4
5	22.4	73.6	68.8	26	13.8	12.96	17.76	27	9.8	21.951	1.33	0.95
6	23	89.2	41.2	33.2	16.2	14.88	15.12	21.6	10.04	23.371	1.23	1.27
7	23.6	48.4	70	26.6	16.08	16.08	17.16	23	5.36	11.282	0.71	1.74
8	24.2	76	67.6	44	17.88	12.24	16.32	24.8	6.2	11.415	0.92	1.2
9	24.8	80.8	88	31.4	12.6	13.32	15	20.4	6.68	14.120	0.89	1.68
10	25.4	53.2	58	21.2	17.64	14.4	13.92	27.8	9.08	22.015	1.56	1.43
11	26	46	97.6	24.8	12.96	15.36	13.68	26.8	8.72	20.836	1.93	1.75
12	26.6	97.6	53.2	29.6	15.72	16.32	16.44	28.6	5.84	8.637	0.62	1.24
13	27.2	66.4	64	28.4	13.92	17.76	12	20.6	8.48	21.743	1.16	2.73
14	27.8	41.2	44.8	38.6	14.64	17.88	15.48	26.2	9.32	21.161	1.19	1.82
15	28.4	90.4	95.2	21.8	16.8	16.8	15.6	23.4	8.6	19.518	1.55	2.49
16	29	42.4	77.2	47	14.4	13.68	16.56	29.6	7.64	17.706	1.3	1.1
17	29.6	71.2	47.2	46.4	13.2	14.76	18	22.2	6.92	13.433	0.67	1.35
18	30.2	78.4	72.4	43.4	17.76	16.2	17.4	28.2	10.28	18.850	2.02	1.9
19	30.8	60.4	65.2	45.2	12	13.92	13.56	24.2	11	25.626	2.8	1.12
20	31.4	40	55.6	34.4	15.12	12.12	14.04	21	7.52	22.087	1.49	1.16
21	32	95.2	66.4	48.8	16.32	17.52	14.16	22	6.56	10.347	0.86	2.23
22	32.6	85.6	56.8	27.8	16.92	14.04	12.12	22.6	5.24	7.961	0.78	1.38
23	33.2	59.2	86.8	36.8	17.16	17.28	13.2	28.8	5.96	10.426	0.94	2
24	33.8	88	52	30.2	14.28	16.56	13.08	29.8	10.52	19.989	1.66	1.66
25	34.4	68.8	83.2	23	14.88	12.36	14.88	29	5.12	8.164	0.76	1.11
26	35	62.8	43.6	20	12.12	15.24	15.24	25	6.8	12.937	0.57	1.13
27	35.6	64	50.8	49.4	17.52	14.52	12.36	25.6	9.44	21.315	2.17	2.89
28	36.2	49.6	76	27.2	14.16	15.84	17.04	20.2	10.64	26.637	2.87	2.72
29	36.8	44.8	80.8	42.8	12.36	17.16	14.64	22.8	5.6	11.522	0.5	2.02
30	37.4	98.8	49.6	39.2	13.32	12	14.52	26.6	7.4	14.451	0.95	0.94
31	38	50.8	100	32	17.28	12.48	15.96	25.4	9.56	22.801	3.69	1.47
32	38.6	84.4	98.8	41	15.24	15.48	17.88	25.2	5.48	7.767	0.8	1.9
33	39.2	92.8	82	45.8	15.6	13.2	16.08	20.8	10.16	23.595	1.51	1.57
34	39.8	79.6	73.6	20.6	14.52	12.72	12.96	23.2	10.4	23.882	2.35	0.86
35	40.4	67.6	94	48.2	14.76	12.84	12.48	24.4	6.44	12.585	1.37	1.67
36	41	96.4	84.4	29	12.72	16.44	12.84	26	6.08	9.191	0.69	1.75
37	41.6	86.8	96.4	38	13.08	13.8	15.72	30	9.92	20.485	2.45	1.54
38	42.2	83.2	60.4	22.4	16.44	13.08	17.64	21.8	7.04	12.690	1.1	1.13
39	42.8	54.4	40	36.2	16.56	14.28	15.84	27.6	5	9.128	0.65	1.16
40	43.4	58	78.4	24.2	15	17.04	17.52	29.4	8.12	17.599	1.27	1.86
41	44	100	61.6	30.8	12.84	16.68	17.28	23.8	9.68	19.872	1.3	1.66
42	44.6	72.4	46	25.4	17.4	18	14.76	23.6	8.36	20.740	1.21	1.85
43	45.2	70	92.8	39.8	15.36	17.4	13.32	24.6	10.76	24.151	3.81	3.02
44	45.8	77.2	59.2	50	13.56	16.92	15.36	29.2	7.16	11.884	0.89	1.85
45	46.4	61.6	42.4	35.6	15.48	13.44	16.68	26.4	10.88	24.204	2.41	1.21
46	47	47.2	71.2	47.6	17.04	15.96	16.8	22.4	7.88	19.538	1.67	2.15
47	47.6	55.6	91.6	23.6	15.84	15.6	13.8	21.2	6.32	12.640	1.19	2.33
48	48.2	43.6	62.8	32.6	14.04	14.64	12.24	28.4	8.24	19.200	1.91	1.23

Table 2 (continued)

Sample	a_{01} (mm)	a_{12} (mm)	a_{23} (mm)	a_{30} (mm)	b_1 (mm)	b_2 (mm)	b_3 (mm)	H (mm)	L (mm)	φ_{fold}	D_1 (mm)	D_2 (mm)
49	48.8	94	74.8	33.8	18	14.16	14.28	28	8	16.180	1.62	1.45
50	49.4	56.8	79.6	35	12.24	12.6	16.92	24	7.28	17.738	1.54	1.21
51	50	74.8	48.4	40.4	13.68	15.12	13.44	20	7.76	18.318	1.09	1.66

The major disadvantage of the Kriging method is that model construction may be time consuming [15, 19, 27]. Fortunately, Lophaven et al. [29, 30] developed a MATLAB Kriging Toolbox (DACE) which facilitates the Kriging metamodeling greatly. Therefore, the Kriging method is applied to develop surrogate models for the folding index and two cavum depths in this work.

3.1 Design of experiment (DOE) by sequential sampling

In metamodeling, the experiment design, i.e., selecting a set of sample points in the design parameter space, is the basic task that must be conducted first. During experiment design, the sampling strategy needs special concern, since it has direct influence on the accuracy of the metamodel. It is generally believed that space-filling designs, including the Latin hypercube design, orthogonal array, minimax and maximin design, entropy design, etc., are preferable for constructing metamodels from deterministic computer experiments such as FE simulation [16, 26]. As is well known, a design for computer experiments should at least satisfy the following two criteria. First, design points should be evenly spread within the design space in order to have a global exploration. On the other hand, the design points should be non-collapsing [31]. To this end, Grosso et al. [32] proposed the space-filling maximin Latin hypercube design (maximin LHD), which is available in the website http://www.spacefillingdesigns.nl. It can make sure the sampling points are evenly spread and non-collapsing within the whole design space. Besides, it offers flexible sample sizes while ensuring stratified sampling and has been widely used for constructing a metamodel. In addition to the sampling approach, the sample size and how to generate the sample points play equally important roles in the accuracy of the metamodel. Typically, sample points are generated all at once or, in other words, at one stage. However, when a limited sample size is affordable, sequentially sampling is preferable. It can take the advantage of information gathered from the existing (earlier calculated) samples, which could be very helpful for identifying an interesting design region and improving the accuracy of the metamodel in the narrowed interesting region. Consider a situation in which we are only interested in a given range of the response; if we simply use the space-filling approach for the entire design space, many sample points will be wasted. By using the sequential sampling approach, the sample points can be added gradually and used to refine the approximation in the interesting region. In addition, the sequential approach requires small computational costs compared to the one-stage sampling approach [26]. Therefore, the maximin LHDs combined with the sequential sampling approach is applied in the present work.

To have a primary global understanding, 51 samples were firstly designed by the maximin LHDs within the whole design space of structural parameters in Table 1. All the samples were simulated with the same processing parameters listed in Table 1. Table 2 gives the detailed experiment schemes and simulation results (φ_{fold}, D_1, and D_2).

Because the objective of this work is to determine the maximum reduction amount (L_{max}) that can satisfy the forming quality requirement, more attention should be paid to the samples with the defect indexes near their corresponding critical values. As mentioned above, the critical value of the folding index is taken as 17.5. On the other hand, Shipley [33] has pointed out that the machining allowance should be less than 3 mm in the precision forging. Thus, the critical values of two cavum depths are set as 3 mm. Figure 5 shows the scatter diagrams of three defect indexes vs. the reduction amount of the above 51 simulation results in Table 2. These figures are helpful for finding the sensitive range of L, in which the defect indexes are close to their critical values. From Fig. 5, it can be seen that φ_{fold} are the most sensitive defect index to L, so the sensitive range of L is determined based on the distribution of φ_{fold}. A wider interval of φ_{fold} containing the critical value (φ_{cr}) is marked by two red dashed lines in Fig. 5a. We can see that plots in the wider interval distribute intensively in the local range of 7–9 mm, which is just the sensitive range of L. Thus, to refine the approximation in this sensitive region, another 21 samples are sequentially designed with L in the range of 7–9 mm while the other parameters still keep the ranges in Table 1. The added samples are also designed by the maximin LHDs, whose detailed schemes and simulation results of defect indexes are given in Table 3.

3.2 Fitting the Kriging metamodel

The mathematical form and constructing method of the Kriging model have been introduced in references [20, 21,

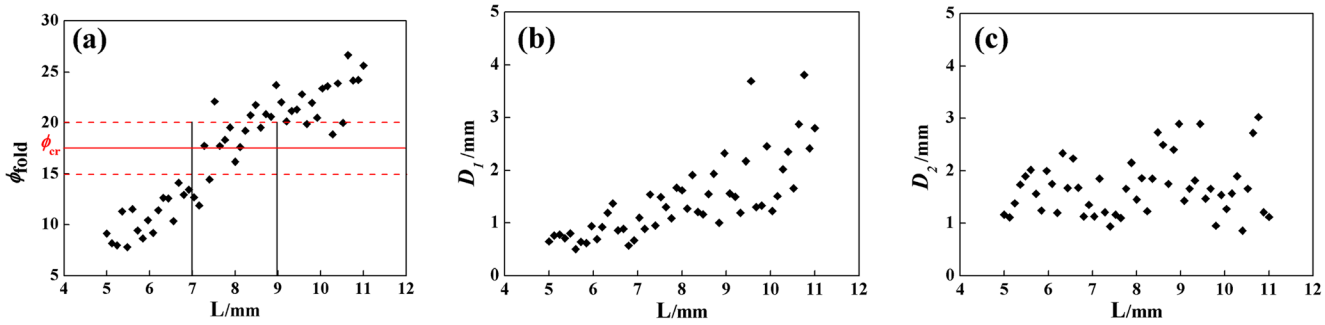

Fig. 5 Defect indexes vs. reduction amount (L) of samples in Table 2: **a** φ_{fold} vs. L; **b** D_1 vs. L; **c** D_2 vs. L

34], which are summarized as below. A Kriging model consists of two parts as shown in Eq. (2). The first part is a linear regression of the data, which models the drift of the process mean over the domain. The second part models systematic deviations from the linear regression, which "pulls" the response surface through the observed data by quantifying the correlation of nearby points.

$$\hat{y}(\mathbf{x}) = \sum_{j=1}^{k} \beta_j f_j(\mathbf{x}) + \mu(\mathbf{x}) \tag{2}$$

In Eq. (2), $\mu(\mathbf{x})$ is a stochastic function with a mean of 0 and variance of σ_μ^2, and whose covariance is shown in Eq. (3).

$$\mathrm{cov}[\mu(\mathbf{v}), \mu(\mathbf{w})] = \sigma_\mu^2 [R(\theta, \mathbf{v}, \mathbf{w})] \tag{3}$$

where $R(\theta,\mathbf{v},\mathbf{w})$ is the spatial correlation function with the general form of

$$R(\theta, \mathbf{v}, \mathbf{w}) = \prod_{j=1}^{n} R_j\left(\theta_j, \left|v_j - w_j\right|\right) \tag{4}$$

Table 3 Simulation schemes and results of 21 sequentially added samples designed by the maximin LHDs

Sample	a_{01} (mm)	a_{12} (mm)	a_{23} (mm)	a_{30} (mm)	b_1 (mm)	b_2 (mm)	b_3 (mm)	H (mm)	L (mm)	φ_{fold}	D_1 (mm)	D_2 (mm)
1	20	76	64	48.5	14.7	17.1	13.2	23	7.9	17.983	0.95	2.44
2	21.5	88	40	36.5	13.8	13.2	17.4	24.5	8.7	19.563	0.82	0.93
3	23	46	55	32	17.1	12.3	14.4	28	7.7	19.463	1.19	0.96
4	24.5	91	70	23	18	15.6	16.8	22.5	7.6	14.779	1.08	1.7
5	26	64	100	21.5	15	16.5	12.6	27	7.4	17.403	1.22	2.33
6	27.5	52	97	39.5	14.4	12.9	15	23.5	9	23.404	2.86	1.69
7	29	58	67	30.5	16.5	17.7	16.5	29.5	8.9	20.926	1.25	1.94
8	30.5	73	82	41	12.9	14.7	17.7	28.5	7.1	13.415	0.84	1.44
9	32	43	52	26	13.2	15.9	16.2	21	7.8	22.665	0.83	1.74
10	33.5	82	46	24.5	12.6	15	12.9	30	8.2	19.606	0.83	1.06
11	35	100	85	27.5	12.3	14.1	14.1	20.5	8	17.075	1.32	1.92
12	36.5	79	61	47	16.2	12	15.6	20	7.3	16.456	1.34	1.19
13	38	97	88	44	16.8	13.8	13.5	29	8.1	15.415	1.66	1.62
14	39.5	40	94	42.5	17.7	16.2	15.9	24	7.5	19.516	1.73	2.08
15	41	67	58	29	17.4	15.3	12.3	21.5	8.8	21.967	1.86	1.99
16	42.5	94	73	45.5	15.6	16.8	18	22	8.6	19.302	1.4	2.12
17	44	49	43	50	14.1	14.4	15.3	27.5	8.4	22.067	1.55	1.51
18	45.5	61	91	38	12	18	13.8	25.5	8.5	19.384	2.03	2.53
19	47	85	49	35	15.9	17.4	14.7	26	7	13.224	0.88	1.78
20	48.5	55	76	33.5	13.5	12.6	12	25	7.2	17.433	1.74	1.23
21	50	70	79	20	15.3	13.5	17.1	26.5	8.3	18.657	1.86	1.25

Table 4 Simulation schemes of 10 additional validation samples designed by the general Latin hypercube design

Sample	a_{01} (mm)	a_{12} (mm)	a_{23} (mm)	a_{30} (mm)	b_1 (mm)	b_2 (mm)	b_3 (mm)	H (mm)	L (mm)
1	34.85	40.347	69.029	43.465	13.077	17.75	13.725	28.839	5.3651
2	35.693	90.117	40.118	34.699	17.374	16.454	16.383	22.213	7.4095
3	45.821	77.633	56.088	24.49	12.314	13.518	17.663	24.683	6.8098
4	21.458	52.059	78.277	39.935	14.328	12.8	15.009	21.629	6.314
5	31.674	64.833	62.991	31.454	15.704	14.66	17.261	27.134	5.9522
6	25.286	83.217	97.017	48.981	14.988	15.136	13.183	23.207	9.8345
7	48.369	95.192	50.257	45.026	16.363	17.148	14.994	25.607	10.621
8	41.056	49.623	72.573	35.869	15.151	14.256	16.073	20.63	8.3789
9	28.464	74.879	89.828	43.465	13.725	12.309	12.249	29.37	9.0306
10	39.334	59.193	83.138	27.602	17.842	15.984	14.099	26.575	9.6156

The correlation function affects the smoothness of the model and the impact of nearby points on the prediction. There are four primary functions commonly used in Kriging: Gaussian, Exponential, Cubic Spline and Matern functions. Gaussian function is the most commonly used in engineering design as it provides a very smooth and infinitely differentiable surface. It is defined with only one parameter to control the range of influence of nearby points. Its form is given by

$$R_j(\theta_j, |v_j - w_j|) = \exp\left(-\theta_j |v_j - w_j|^2\right) \tag{5}$$

Let the set of known training samples $\mathbf{X}=[\mathbf{x}_1,\mathbf{x}_2,\cdots,\mathbf{x}_n]$ and its response $\mathbf{Y}=[y(\mathbf{x}_1),y(\mathbf{x}_2),\cdots,y(\mathbf{x}_n)]$. The estimator of response of any sample $\mathbf{x}$ is

$$\widehat{y}(\mathbf{x}) = \mathbf{f}^T(\mathbf{x})\widehat{\boldsymbol{\beta}} + \mathbf{r}^T(\mathbf{x})\mathbf{R}^{-1}\left(\mathbf{Y} - \mathbf{F}\widehat{\boldsymbol{\beta}}\right) \tag{6}$$

where

$$\mathbf{F} = \left[\mathbf{f}(\mathbf{x}_1), \mathbf{f}(\mathbf{x}_2), \cdots, \mathbf{f}(\mathbf{x}_n)\right]^T \tag{7}$$

$$\mathbf{r}^T(\mathbf{x}) = \left[\mathbf{R}(\mathbf{x},\mathbf{x}_1), \mathbf{R}(\mathbf{x},\mathbf{x}_2), \cdots, \mathbf{R}(\mathbf{x},\mathbf{x}_n)\right] \tag{8}$$

$$\mathbf{R} = \left[\mathbf{r}^T(\mathbf{x}_1), \mathbf{r}^T(\mathbf{x}_2), \cdots, \mathbf{r}^T(\mathbf{x}_n)\right]^T \tag{9}$$

$$\widehat{\boldsymbol{\beta}} = \left(\mathbf{F}^T\mathbf{R}^{-1}\mathbf{F}\right)^{-1}\mathbf{F}^T\mathbf{R}^{-1}\mathbf{Y} \tag{10}$$

The estimator of process variance is given by

$$\widehat{\sigma}_\mu^2 = \left(\mathbf{Y} - \mathbf{F}\widehat{\boldsymbol{\beta}}\right)^T\mathbf{R}^{-1}\left(\mathbf{Y} - \mathbf{F}\widehat{\boldsymbol{\beta}}\right)/n \tag{11}$$

At last, the regression function coefficients, process variance, and correlation function parameter θ_j for the Kriging metamodel are usually estimated by maximum likelihood estimation (MLE).

As mentioned above, Lophaven et al. [29, 30] developed a MATLAB Kriging Toolbox (DACE) for Kriging metamodeling. It can easily estimate the correlation functions and the corresponding optimal weights. Besides, it is well documented and free of charge (http://www.imm.dtu.dk/~hbni/dace/) and has been widely used in Kriging

Table 5 Comparisons of the FE simulation and Kriging prediction results of 10 validation samples

Sample	φ_{fold}			D_1 (mm)			D_2 (mm)		
	FE	Kriging	Error (%)	FE	Kriging	Error (%)	FE	Kriging	Error (%)
1	11.07	9.765	11.78	0.63	0.703	11.63	1.54	1.674	8.71
2	15.808	15.258	3.48	0.91	0.928	1.98	1.32	1.530	15.91
3	12.868	12.417	3.50	0.72	0.835	15.94	1	1.007	0.72
4	16.452	14.573	11.42	0.97	0.932	3.96	1.36	1.422	4.58
5	10.75	10.672	0.73	0.75	0.738	1.66	1.27	1.080	14.94
6	21.597	21.892	1.37	2.33	2.295	1.51	2.53	2.577	1.87
7	20.033	21.649	8.06	2.18	2.000	8.24	2.1	2.088	0.55
8	23.029	21.915	4.83	2.05	1.975	3.65	2.19	1.935	11.66
9	18.403	20.942	13.80	1.95	1.814	6.99	1.27	1.291	1.66
10	22.885	21.655	5.38	2.75	2.519	8.39	2.24	2.183	2.56

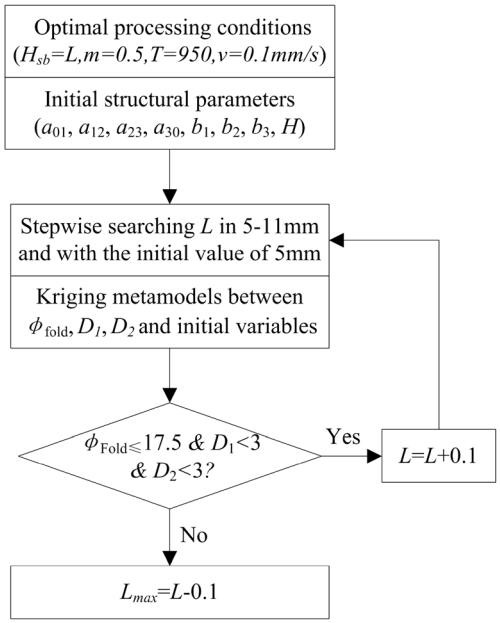

Fig. 6 Flow chart of determination of forming limit for local loading forming considering defects in transitional region through stepwise searching combined with Kriging metamodels

metamodeling. Thus, DACE was used to establish Kriging metamodels of three defect indexes here. Three Kriging metamodels of φ_{fold}, D_1, and D_2 are developed, respectively, based on all the sample data in Tables 2 and 3. For the Kriging metamodel of φ_{fold}, the regression model takes the first-order polynomial and its determined correlation function parameter (theta) is 2. As for the Kriging metamodels of D_1 and D_2, the regression models both take the zero-order polynomial and their determined correlation function parameters are 2.9 and 0.3, respectively.

3.3 Kriging metamodel validation

Since the Kriging metamodel interpolates the sample data, additional validation points are designed to assess the accuracy of each metamodel. Ten additional random samples are designed within the whole design space in Table 1 by general the Latin Hypercube design through MATLAB software, as listed in Table 4. Table 5 shows the comparisons of FE simulation and Kriging prediction results.

To provide a more complete picture of the metamodel accuracy, the average absolute error (AAE) and correlation determination (R^2) are computed. The equations of these two measures are given in Eqs. (12) and (13).

$$\mathrm{AAE} = \frac{1}{n}\sum_{i=1}^{n}\left|\frac{y_i-\hat{y}_i}{y_i}\right| \tag{12}$$

$$R^2 = 1-\frac{\sum_{i=1}^{n}(y_i-\hat{y}_i)^2}{\sum_{i=1}^{n}(y_i-\bar{y})^2} \tag{13}$$

where n is the number of validation points, $\hat{y}_i$ is the predicted value for the observed value y_i, and $\bar{y}$ is the mean of the observed values at validation points. The AAE of φ_{fold}, D_1, and D_2 are 6.43, 6.39, and 6.32 %, respectively. The R^2 of φ_{fold}, D_1, and D_2 are 0.910, 0.977, and 0.931, respectively. The above results suggest that three developed Kriging metamodels of φ_{fold}, D_1, and D_2 are all reliable to predict the defect indexes of the transitional region instead of FE simulation.

4 Determination of the forming limit based on the Kriging metamodel

As mentioned above, stepwise searching with a small interval is a very easy and effective method to determine the forming limit. And, the efficiency of stepwise searching is determined by the efficiency of response acquisition at any sample point. It has been described that the defect responses of any sample can be predicted quickly and accurately through the established Kriging metamodels in Section 3. Therefore, in this section, the forming limit for local loading forming considering defects in the transitional region is determined using the stepwise searching method based on Kriging metamodels of defect indexes.

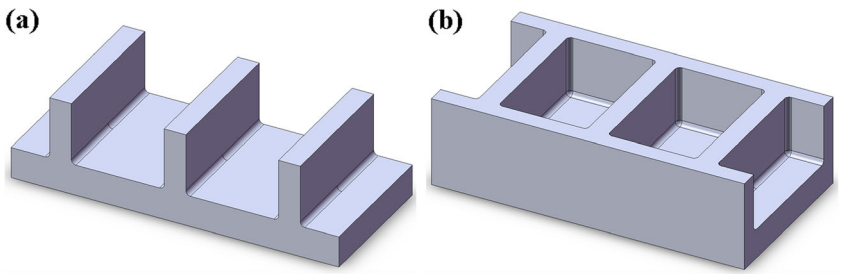

Fig. 7 Schematic of two transitional region models: **a** without transverse rib; **b** with transverse rib

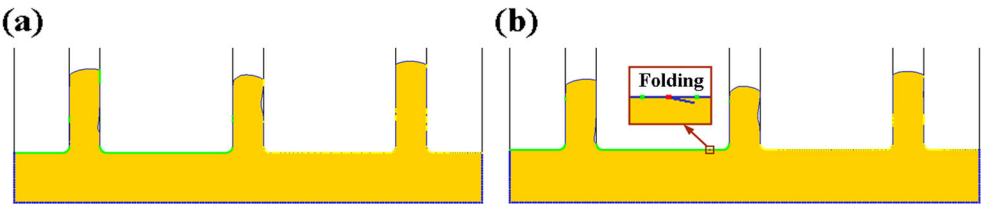

Fig. 8 Forming results of transitional region model without transverse rib at reduction amounts of **a** 7.5 mm and **b** 7.6 mm

4.1 Determination method

Figure 6 shows the flow chart of determination of the forming limit through stepwise searching combined with the Kriging metamodel. Considering the forming quality, the optimal local loading processing conditions presented in Table 1 are taken in this work, which was described in Section 2. The initial structural parameters of the transitional region model should be extracted according to the geometry of the objective component. Then, the stepwise searching for L_{max} is conducted in the range of 5–11 mm with the initial value of 5 mm and step size of 0.1 mm. In any searching step, input the initial structural parameters and current L_n into the developed Kriging metamodels to get the predictedφ_{fold}, D_1, and D_2, respectively. Subsequently, compare the relationship between predicted defect indexes and their corresponding critical values. As described above, the critical values of φ_{fold}, D_1, and D_2 are set as 17.5, 3 mm, and 3 mm, respectively. If all three predicted defect indexes are smaller than their corresponding critical values, set $L_{n+1}=L_n+0.1$ and proceed to the next step; else the L_{max} is determined as $L_n-0.1$. According to the above steps, L_{max} can be determined, which would be demonstrated and validated in the next subsection.

4.2 Application and validation

In this subsection, the above method is applied to determine the forming limits of two transitional region models to validate its reliability. Figure 7 shows the schematic of two objective transitional region models. Two models have different geometry features on the transverse rib, but their symmetry plans present the same 2D structural parameters shown in Fig. 3. The structural parameters a_{01}, a_{12}, a_{23}, a_{30}, b_1, b_2, b_3, and H are 25, 60, 60, 25, 14, 14, 14, and 30 mm, respectively. And the fillet radiuses are both 3 mm for two objective models. Through the above method, it is predicted that the two models have the same forming limit with L_{max}=7.5 mm due to their same structural parameters.

To verify the predicted L_{max}, FE simulations of the local loading forming of the two objective models are conducted. For the model without the transverse rib (Fig. 7a), 2D FE simulations are carried out with L near the predicted L_{max} (7.5 mm). The forming results with L of 7.5 and 7.6 mm are shown in Fig. 8 as examples. It can be found from Fig. 8a that when L is 7.5 mm, no folding defect generates and D_1 and D_2 are 0.93 and 1.15 mm, respectively. Nevertheless, when L is 7.6 mm, the folding defect generates at the stroke of 6.655 mm, as shown in Fig. 8b. All simulation results show that when L is ≤7.5 mm, no folding defect generates, and D_1 and D_2 are both smaller than 3 mm, presenting a qualified forming result. However, when L is >7.5 mm, the folding defect generates. It suggests that the above method is applicable to determine the forming limit of the transitional region model without the transverse rib. For the model with the transverse rib, 3D FE simulations, whose model was developed and verified in [12], are carried out with L near 7.5 mm. The forming results with L of 7.5 and 7.7 mm are shown in Fig. 9 as examples. To clarify, the sample with L of 7.6 mm produces very small folding, which is not shown as example. All simulation results show that when L is ≤7.5 mm, no folding defect generates, and D_1 and D_2 are both smaller than 3 mm, presenting a qualified forming result. However, when L is >7.5 mm, the folding defect generates. It suggests that the forming limit for the model with the transverse rib is also consistent with the predicted L_{max} (7.5 mm). Above, it can be concluded that the stepwise searching method based on Kriging metamodels of defect indexes is an effective and reliable method to determine the forming limit for local loading forming considering defects in the transitional region. And the method presents a certain commonality for different transitional region models without or with the transverse rib.

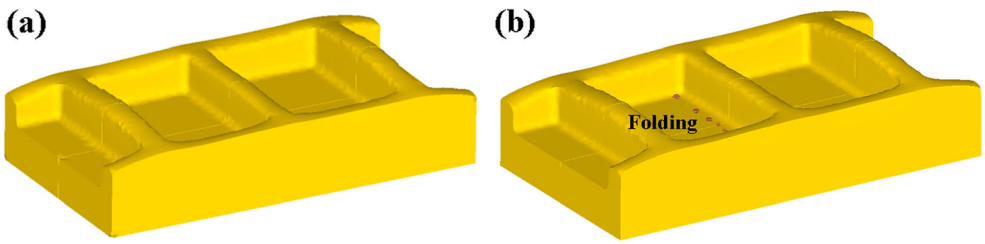

Fig. 9 Forming results of transitional region model with transverse rib at reduction amounts of **a** 7.5 mm and **b** 7.7 mm

5 Conclusions

In this paper, the forming limit (maximum reduction amount) and its determination method in local loading forming of a large-scale rib-web component considering defects in the transitional region was investigated. The following conclusions can be drawn:

1. In metamodeling, the space-filling maximin Latin hypercube designs (maximin LHDs) and sequential sampling approach were employed to design sample points, which can guarantee the accuracy of the metamodel in global design space and improve the accuracy of the metamodel in the interesting critical region.
2. The Kriging metamodels of defect indexes in the transitional region were developed based on the FE simulation results of designed samples with various structural parameters, and verified by ten extra random samples designed within the global design space. The developed Kriging metamodels can predict the defect indexes in the transitional region quickly and accurately.
3. The method of determining the forming limit, stepwise searching combined with the developed Kriging metamodels, was proposed and successfully applied to two specific transitional region models. Application results indicate that the proposed method is an effective and reliable method to determine the forming limit considering defects in the transitional region during local loading forming of titanium alloy large-scale rib-web components.

Acknowledgments The authors would like to gratefully acknowledge the support of the National Natural Science Foundation of China for Key Program (No. 50935007), National Basic Research Program of China (No. 2010CB731701), National Natural Science Foundation of China (No. 51205317), 111 Project (B08040), Excellent Doctorate Foundation of Northwestern Polytechnical University, the Open Research Fund of State Key Laboratory of Materials Processing and Die & Mould Technology, Huazhong University of Science and Technology, and the Research Fund of the State Key Laboratory of Solidification Processing (NWPU), China (Grant No. 104-QP-2014).

References

1. Shen G, Furrer D (2000) Manufacturing of aerospace forgings. J Mater Process Technol 98:189–195
2. Zhang DW, Yang H, Sun ZC, Fan XG (2012) Deformation behavior of variable-thickness region of billet in rib-web component isothermal local loading process. Int J Adv Manuf Technol 63(1–4):1–12
3. Zhang DW, Yang H (2013) Metal flow characteristics of local loading forming process for rib-web component with unequal-thickness billet. Int J Adv Manuf Technol 68(9–12):1949–1965
4. Zhang DW, Yang H, Sun ZC (2010) Analysis of local loading forming for titanium-alloy T-shaped components using slab method. J Mater Process Technol 210:258–266
5. Zhang DW, Yang H (2013) Preform design for large-scale bulkhead of TA15 titanium alloy based on local loading features. Int J Adv Manuf Technol 67:2551–2562
6. Sun ZC, Yang H (2009) Microstructure and mechanical properties of TA15 titanium alloy under defects-step local loading forming. Mater Sci Eng A 523(1–2):184–192
7. Fan XG, Yang H, Sun ZC, Zhang DW (2010) Effect of deformation inhomogeneity on the microstructure and mechanical properties of large-scale rib-web component of titanium alloy under local loading forming. Mater Sci Eng A 527:5391–5399
8. Gao PF, Yang H, Fan XG (2014) Quantitative analysis of the material flow in transitional region during isothermal local loading forming of Ti-alloy rib-web component. Int J Adv Manuf Technol 75(9–12):1339–1347
9. Zhang DW, Yang H (2013) Numerical study of the friction effects on the metal flow under local loading way. Int J Adv Manuf Technol 68:1339–1350
10. Zhang DW, Yang H, Sun ZC, Fan XG (2011) Deformation behavior under die partitioning boundary during titanium alloy large-scale rib-web component forming by isothermal local loading. Proceedings of the 12th World Conference on Titanium. Science Press, Beijing, p 328
11. Zhang DW, Yang H (2014) Distribution of metal flowing into unloaded area in the local loading process of titanium alloy rib-web component. Rare Metal Mater Eng 43(2):296–300
12. Gao PF, Yang H, Fan XG, Lei PH (2014) Forming defects control in transitional region during isothermal local loading of Ti-alloy rib-web component. Int J Adv Manuf Technol 76(5–8):857–868
13. Chen FK, Huang TB, Wang SJ (2007) A study of flow-through phenomenon in the press forging of magnesium-alloy sheets. J Mater Process Technol 187–188:770–774
14. Sun ZC, Yang H (2007) Study on forming limit and feasibility of tube axial compressive process. J Mater Process Technol 187–188: 292–295
15. Wang GG, Shan S (2006) Review of metamodeling techniques in support of engineering design optimization. J Mech Des 129(4): 370–380
16. Chen V, Tsui KL, Barton RR, Meckesheimer M (2006) A review on design, modeling and applications of computer experiments. IIE Trans 38(4):273–291
17. Guan Y, Bai X, Liu M, Song L, Zhao G (2015) Preform design in forging process of complex parts by using quasi-equipotential field and response surface methods. Int J Adv Manuf Technol. doi:10.1007/s00170-014-6775-6
18. Kleijnen J (2009) Kriging metamodeling in simulation: a review. Eur J Oper Res 192:707–716
19. Beers W, Kleijnen J (2004) Kriging interpolation in simulation: a survey. Proceedings of the 2004 Winter Simulation Conference
20. Martin JD, Simpson TW (2003) A study on the use of Kriging models to approximate deterministic computer models. Proceedings of DETC'03 ASME 2003 Design Engineering Technical Conferences and Computers and Information in Engineering Conference, Chicago, September 2–6
21. Martin JD, Simpson TW (2004) On the use of Kriging models to approximate deterministic computer models. Proceedings of DETC'04: ASME 2004 International Design Engineering Technical Conferences and Computers and Information in Engineering Conference, Salt Lake City, September 28 - October 2
22. Gao PF, Yang H, Fan XG, Lei PH (2015) Quick prediction of the folding defect in transitional region during isothermal local loading forming of titanium alloy large-scale rib-web component based on folding index. J Mater Process Technol 219:101–111
23. Shen CW (2007) Research on material constitution models of TA15 and TC11 titanium alloys in hot deformation process. Master Thesis, Northwestern Polytechnical University

24. Guo HZ (2009) Forging of alloy steel and nonferrous alloy, 2nd edn. Northwestern Polytechnical University Press, Xi'an, pp 220–256 (in Chinese)
25. Simpson TW, Lin D, Chen W (2001) Sampling strategies for computer experiments: design and analysis. Int J Reliab Appl 2(3):209–240
26. Jin R, Chen W, Sudjianto A (2002) On sequential sampling for global metamodeling in engineering design. Proceedings of DETC'02: ASME 2002 Design Engineering Technical Conferences And Computers and Information in Engineering Conference. Montreal, September 29-October 2
27. Jin R, Chen W, Simpson TW (2001) Comparative studies of metamodeling techniques under multiple modeling criteria. Struct Multidiscip Optim 23(1):1–13
28. Simpson TW (1998) Comparison of response surface and Kriging models in the multidisciplinary design of an aerospike nozzle. Langley Research Center, NASA NASA/CR-1998-206935, Hampton, VA, February
29. Lophaven SN, Nielsen HB, Sondergaard J (2002) DACE: a Matlab Kriging toolbox, version 2.0. IMM Technical University of Denmark, Lyngby. ISBN DACE: a Matlab Kriging toolbox
30. Kleijnen J, Van BW, Van NI (2010) Constrained optimization in expensive simulation: novel approach. Eur J Oper Res 202(1):164–174
31. Rennen G, Husslage B, Dam ER, Hertog DD (2009) Nested maximin Latin hypercube designs. ISSN 0924–7815, No. 2009–06
32. Grosso A, Jamali A, Locatelli M (2009) Finding maximin Latin hypercube designs by Iterated Local Search heuristics. Eur J Oper Res 197(2):541–547
33. Shipley RJ (1988) Precision forging, forging process, ASM Handbook. ASM International, USA
34. Ge XW, Han XH, Chen W, Zhou XH (2010) Processing parameters optimization based on Kriging metamodel for gas-assisted injection molding. J Chem Ind Eng 61(4):909–915 (in Chinese)